

Imaging of glioma tumor with endogenous fluorescence tomography

Dax S. Kepshire,^a Summer L. Gibbs-Strauss,^a Julia A. O'Hara,^{a,d} Michael Hutchins,^b Nicolae Mincu,^b Frederic Leblond,^a Mario Khayat,^b Hamid Dehghani,^c Subhadra Srinivasan,^a and Brian W. Pogue^{a,*}

^aDartmouth College, Thayer School of Engineering, Hanover, New Hampshire 03755

^bART Advanced Research Technologies Inc, Saint-Laurent, Quebec, Canada H4S 2A4

^cUniversity of Exeter, School of Physics, Stocker Road, Exeter, EX4 4QL, United Kingdom

^dDartmouth Medical School, Department of Diagnostic Radiology, Hanover, New Hampshire 03755

Abstract. Tomographic imaging of a glioma tumor with endogenous fluorescence is demonstrated using a non-contact single-photon counting fan-beam acquisition system interfaced with microCT imaging. The fluorescence from protoporphyrin IX (PpIX) was found to be detectable, and allowed imaging of the tumor from within the cranium, even though the tumor presence was not visible in the microCT image. The combination of single-photon counting detection and normalized fluorescence to transmission detection at each channel allowed robust imaging of the signal. This demonstrated use of endogenous fluorescence stimulation from aminolevulinic acid (ALA) and provides the first *in vivo* demonstration of deep tissue tomographic imaging with protoporphyrin IX. © 2009 Society of Photo-Optical Instrumentation Engineers. [DOI: 10.1117/1.3127202]

Keywords: fluorescence; fluorescence molecular tomography; tomography.

Paper 08340LRR received Sep. 19, 2008; revised manuscript received Mar. 9, 2009; accepted for publication Mar. 10, 2009; published online May 11, 2009; corrected May 20, 2009.

Fluorescence tomography provides a tool for preclinical molecular contrast agent assessment in oncology.¹⁻⁴ Systems have advanced in complexity to where noncontact imaging,⁵ automated boundary recovery,⁶ and sophisticated internal tissue shapes can be included in the recovered images. The translation of this work to humans will require molecular contrast agents that are amenable to regulatory approval and maintain tumor specificity in humans, where often nonspecific uptake of molecular imaging agents can decrease their utility. In this study, a new fluorescence tomography system coupled to microCT⁷ was used to illustrate diagnostic detection of orthotopic glioma tumors that were not apparent in the microCT images, using endogenous fluorescent contrast from protoporphyrin IX (PpIX).

Glioma tumors provide significant endogenous fluorescence from PpIX,⁸⁻¹¹ and this is enhanced when the subject imaged has been administered aminolevulinic acid (ALA). The endogenous production process of PpIX is known to stem from the administered, ALA bypassing the regulatory inhibi-

tion of ALA synthase, allowing the heme synthesis pathway to proceed uninhibited. Since there is a limited supply of iron in the body, this process produces overabundance of PpIX rather than heme, and many tumors have been shown to have high yields of PpIX. Clinical trials with PpIX fluorescence guided resection of tumors have shown significant promise,¹² and yet deep tissue imaging with PpIX fluorescence has not been exploited in clinical use. Early studies have shown that detection of these tumors with PpIX is feasible,^{13,14} but no tomographic imaging has been used. This limitation in development has largely been caused by problems in wavelength filtering and low signal intensity, as well as background fluorescence from the skin limiting sensitivity to deeper structures. In the system developed and used here, this feasibility is demonstrated by imaging a human xenograft glioma model.

To solve the sensitivity problem and study the ability to diagnostically image PpIX *in vivo*, time-correlated single-photon counting was used in the fluorescence tomography system, which provides maximum sensitivity. Figure 1(a) shows the system designed to match up with a microCT, allowing both x-ray structural and optical functional imaging sequentially. Lens-coupled detection of signals is acquired from the mouse using five time-resolved photomultiplier tubes (H7422P-50, Hamamatsu, Japan) with single-photon counting electronics (SPC-134 modules, Becker and Hickl GmbH, Germany). The system has fan-beam transmission geometry similar to a standard CT scanner, with single source delivery of a 1-mW pulsed diode laser light at 635 nm, collimated to a 1-mm effective area on the animal. The five detection lenses were arranged in an arc, each with 22.5-deg angular separation, centered directly on the opposite side of the animal with long working distance pickup,¹ allowing non-contact measurement of the diffuse light through the animal. The diffuse intensity signals collected at each of the five channels were then translated via 400- μ m fibers and split using beamsplitters to be directed toward the fluorescence (95%) and transmission (5%) channel detectors. A 650-nm long-pass filter was used in the fluorescence channels to isolate the signal, and in the transmitted intensity signals, a neutral density filter (2 OD) was used to attenuate the signals. This latter filtering was necessary to ensure that the fluorescence and transmission. Intensity signals fell within the same dynamic range, allowing a single 1 s acquisition for each detector. Scans were then performed by rotating the fan-beam around the specimen to 32 locations. A GE eXplore Locus SP scanner (GE Healthcare, London, Ontario, Canada) that incorporated a detector with 94-micron pixel resolution, a 80-kV peak voltage, and a tube current of 450 μ As, was used in acquiring the microCT data, as displayed in Fig. 2. In this example, since soft tissue was being imaged, the CT data was largely used to image the exterior of the animal, although in future studies, it could be used to isolate the cranium region as well.

Calibration of the fluorescence tomography system was carried out with standard tissue-simulating epoxy resin phantoms with tissue-like scatter and absorption coefficients. The details of the calibration procedure have been reported previously^{7,15-17} and a single phantom is shown here to illustrate the type of data, as shown in Fig. 1(b). The phantom contained an 8-mm liquid inclusion filled with 1 μ g/ml

*Address all correspondence to: Brian W. Pogue. Tel: 603 646-3861; E-mail: pogue@dartmouth.edu

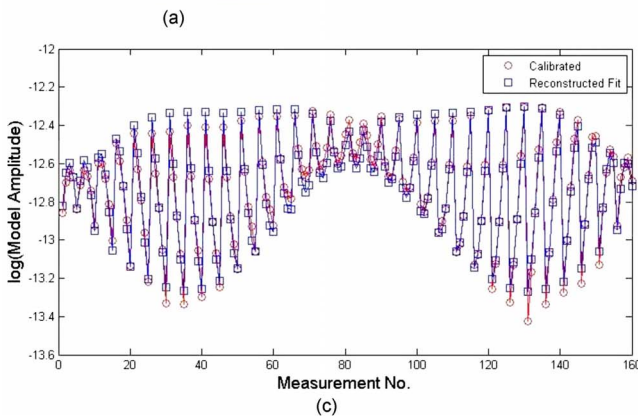
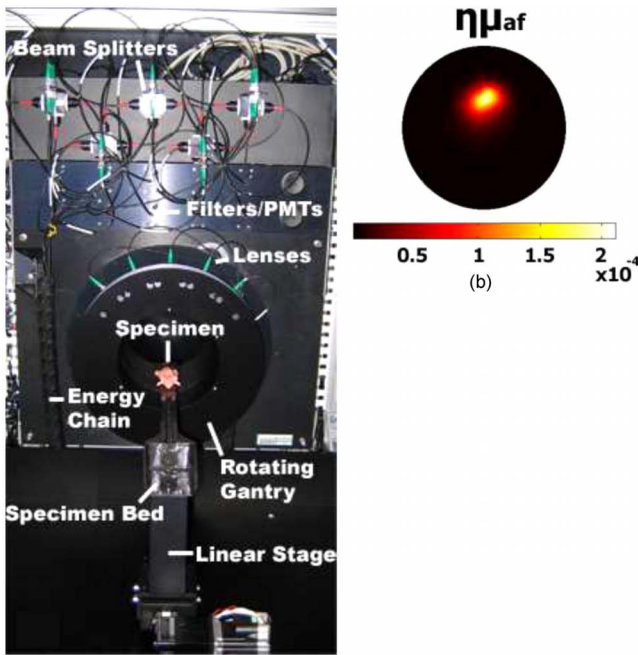


Fig. 1 (a) Photograph of the fluorescence tomography system, with the main components labeled. (b) A tomography dataset as measured through a tissue phantom—the reconstructed image data is overlaid on this. (c) The recovered image from the phantom.

PpIX. This concentration is similar to that seen in malignant gliomas.^{12–14} Experimental datasets were then calibrated into the fluorescence-to-transmission signal ratio at each detection location, and then the signal was scaled such that the average ratio matched that of the model.^{16,18} In Fig. 1(c), the calibrated dataset used to generate this image is shown along with the reconstructed fit, illustrating convergence of this dataset with near infrared fluorescence, absorption and scatter tomography (NIRFAST) finite-element-based nonlinear reconstruction.^{17,19} The system noise was determined at SNR of 1.1% in the raw fluorescence-to-transmission data, as assessed by repeated samplings of a stable signal. This level is acceptable for reconstruction of the fluorescence yield and consistent with levels seen in previous diffuse tomography systems. The concentration of PpIX in the phantom was increased over ranges expected in tissue, and the images were reconstructed. The value in the region of interest was extracted and plotted in Fig. 3.

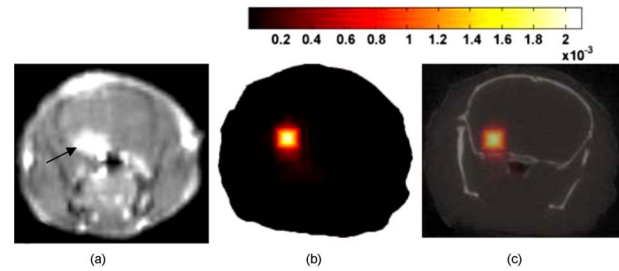


Fig. 2 (a) Image of the rodent glioma tumor, as viewed by contrast magnetic resonance imaging. (b) The fluorescence tomography image of PpIX, and (c) the overlay of this image onto the microCT image of the cranium slice.

The animal model was the U251 xenograft glioma line, grown in the laboratory for ongoing detection studies and published extensively^{13,14} and is known to have high PpIX levels. The experimental plan was approved by the Institutional Animal Care and Use Committee. Briefly, 10^6 cells were stereotactically implanted into the brain in $10 \mu\text{L}$ of PBS through a Hamilton syringe, through a 1-mm hole in the skull. Tumors were implanted 2 mm deep into the brain with injection over 5 min. The tumor was incubated for 14 days and imaged *in vivo* with contrast magnetic resonance to assess size and location. Figure 2(a) shows a gadolinium-enhanced T1 weighted image of the tumor. A microCT dataset was then acquired and an exposure time of 100 ms was used, with three repeated measurements at each of the 400 gantry angles, for a total acquisition time of 11 min. The mouse bed to hold the animal was the original microCT carbon fiber bed supplied by GE, with slots cut to allow optical measurement laterally across the cranium. After CT imaging, the animal and bed were positioned in the fluorescence tomography system, and a pre-ALA-injection dataset was acquired with 64 angles using integration time of 4 s per angle, with a 10-min total acquisition. Following administration of ALA and incubation

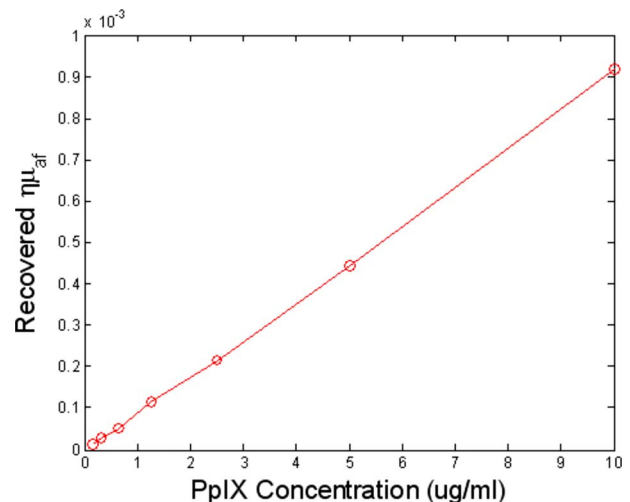


Fig. 3 The reconstructed quantum yield multiplied by the fluorophore absorption coefficient is shown within the region of the phantom, for a range of increasing PpIX concentrations. The linearity of the recovery provides a reliable way to calibrate the concentration from within tomographic images.

over 1 h, the animal was reimaged using the fluorescence scanner, and a post-contrast dataset was generated. The external boundary representing the cranium in the 2-D region of interest was then segmented and used to create a finite element mesh²⁰ for fluorescence tomography reconstruction. The contour information from the microCT allowed calculation of source and detector locations in an automated fashion.

The peak Q-band excitation for PpIX is known to be at 635-nm wavelength excitation with a molar absorption coefficient near $10^4 \text{ M}^{-1} \text{ cm}^{-1}$, which is why the system designed here used this laser for excitation. The peak of the emission is near 640 nm, which would be challenging to detect with 635-nm excitation because of the problems in filtering. However, it has a long emission tail with a second peak out near 700 nm, allowing effective fluorescence detection with the 650-nm long-pass filters designed into the system. The fluorescence quantum yield of this compound is estimated to be near 0.5% (Ref. 16). The fluorescence-to-transmission ratio data was calibrated as in the phantom study and reconstructed to create the image in Fig. 2(b). This was then superimposed on the microCT image, as shown in Fig. 2(c), to create a hybrid structural functional image of the endogenous fluorescence contrast. The microCT image did not show any evidence of the tumor, and prior studies with injected contrast did not show any promise of visualizing this intracranial tumor, due to the inherent soft tissue contrast limitations of microCT imaging. Recovery of the spatial distribution of fluorescence yield was robust, however, and indicates an effective PpIX concentration near $10 \mu\text{g/ml}$. This value is based on the phantom calibration curve, although exact quantitative recovery of tomographic images must be interpreted carefully with validation by similar-sized objects in similar positions to the true case.

In summary, this paper presents initial evidence that non-invasive tomography of tumors with PpIX fluorescence can be achieved, using noncontact near-infrared signal measurement. The most important factor in being able to achieve this imaging was the use of single-photon counting, which allowed imaging through deep tissue in a reasonable time frame. Another important factor was the use of ratio data of the fluorescence-to-transmission signals, acquired simultaneously, because this ratio is resistant to many calibration errors, distance inaccuracies, or tissue heterogeneity. The exterior boundary from microCT provided higher accuracy in localization of the reconstructed volume, and so the combination of microCT and fluorescence tomography was beneficial. Further use of interior structures from microCT imaging could also enhance the localization and quantitative estimation of fluorescence *in vivo*.

Acknowledgments

This work was funded by NIH Research Grant No. R01CA120368 and by ART, Inc.

References

1. V. Ntziachristos, C. H. Tung, C. Bremer, and R. Weissleder, "Fluorescence molecular tomography resolves protease activity *in vivo*," *Nat. Med.* **8**(7), 757–760 (2002).
2. H. K. Choi, D. Yessayan, H. J. Choi, E. Schellenberger, A. Bogdanov, L. Josephson, R. Weissleder, and V. Ntziachristos, "Quantitative analysis of chemotherapeutic effects in tumors using *in vivo* staining and correlative histology," *Cellular Oncol.* **27**(3), 183–190 (2005).

3. V. Ntziachristos, E. A. Schellenberger, J. Ripoll, D. Yessayan, E. Graves, A. Bogdanov Jr., L. Josephson, and R. Weissleder, "Visualization of antitumor treatment by means of fluorescence molecular tomography with an annexin V-Cy5.5 conjugate," *Proc. Natl. Acad. Sci. U.S.A.* **101**(33), 12294–12299 (2004).
4. V. Ntziachristos, "Fluorescence molecular imaging," *Annu. Rev. Biomed. Eng.* **8**, 1–33 (2006).
5. N. Deliolanis, T. Lasser, D. Hyde, A. Soubret, J. Ripoll, and V. Ntziachristos, "Free-space fluorescence molecular tomography utilizing 360 degree geometry projections," *Opt. Lett.* **32**(4), 382–384 (2007).
6. H. Meyer, A. Garofalakis, G. Zacharakis, S. Psycharakis, C. Marmalaki, D. Kioussis, E. N. Economou, V. Ntziachristos, and J. Ripoll, "Noncontact optical imaging in mice with full angular coverage and automatic surface extraction," *Appl. Opt.* **46**(17), 3617–3627 (2007).
7. D. Kepshire, N. Mincu, M. Hutchins, J. Gruber, H. Dehghani, J. Hynarowski, F. Leblond, M. Khayat, and B. W. Pogue, "A microCT guided fluorescence tomography system for small animal molecular imaging," *Rev. Sci. Instrum.* **80**, 043701 (2009).
8. J. C. Kennedy and R. H. Pottier, "Endogenous protoporphyrin IX, a clinically useful photosensitizer for photodynamic therapy," *J. Photochem. Photobiol., B* **14**(4), 275–292 (1992).
9. M. Kriegmair, R. Baumgartner, R. Knuechel, P. Steinbach, A. Ehsan, W. Lumper, F. Hofstadter, and A. Hofstetter, "Fluorescence photodetection of neoplastic urothelial lesions following intravesical instillation of 5-aminolevulinic acid," *Urology* **44**(6), 836–841 (1994).
10. R. Cubeddu, G. Canti, P. Taroni, and G. Valentini, "Delta-aminolevulinic acid induced fluorescence in tumor-bearing mice," *J. Photochem. Photobiol., B* **30**(1), 23–27 (1995).
11. S. L. Marcus, R. S. Sobel, A. L. Golub, R. L. Carroll, S. Lundahl, and D. G. Shulman, "Photodynamic therapy (PDT) and photodiagnosis (PD) using endogenous photosensitization induced by 5-aminolevulinic acid (ALA): current clinical and development status," *J. Clin. Laser Med. Surg.* **14**(2), 59–66 (1996).
12. W. Stummer, U. Pichlmeier, T. Meinel, O. D. Wiestler, F. Zanella, H.-J. Reulen, and A.L.-G.S. Group, "Fluorescence-guided surgery with 5-aminolevulinic acid for resection of malignant glioma: a randomised controlled multicentre phase III trial. [see comment]," *Lancet Oncol.* **7**(5), 392–401 (2006).
13. S. L. Gibbs-Strauss, J. A. O'Hara, P. J. Hoopes, T. Hasan, and B. W. Pogue, "Noninvasive measurement of aminolevulinic acid-induced protoporphyrin IX fluorescence allows detection of glioma *in vivo*," *J. Biomed. Opt.* **14**(1), 014007 (2009).
14. S. L. Gibbs-Strauss, J. A. O'Hara, S. Srinivasan, P. J. Hoopes, T. Hasan, and B. W. Pogue, "Diagnostic detection of diffuse glioma tumors *in vivo* with molecular fluorescence transmission from endogenous proteins," *Med. Phys.* **36**(3), 974–983 (2009).
15. V. Ntziachristos, X. H. Ma, and B. Chance, "Time-correlated single photon counting imager for simultaneous magnetic resonance and near-infrared mammography," *Rev. Sci. Instrum.* **69**(12), 4221–4233 (1998).
16. S. C. Davis, R. Springett, C. Leussler, P. Mazurkewitz, S. Tuttle, S. L. Gibbs-Strauss, H. Dehghani, B. W. Pogue, and K. D. Paulsen, "Magnetic resonance-coupled fluorescence tomography scanner for molecular imaging of small animals and human breasts," *Rev. Sci. Instrum.* **79**, 064302 (2008).
17. D. S. Kepshire, S. C. Davis, H. Dehghani, K. D. Paulsen, and B. W. Pogue, "Subsurface diffuse optical tomography can localize absorber and fluorescent objects but recovered image sensitivity is nonlinear with depth," *Appl. Opt.* **46**(10), 1669–1678 (2007).
18. V. Ntziachristos, G. Turner, J. Dunham, S. Windsor, A. Soubret, J. Ripoll, and H. A. Shih, "Planar fluorescence imaging using normalized data," *J. Biomed. Opt.* **10**(6), 064007 (2005).
19. S. C. Davis, H. Dehghani, J. Wang, S. Jiang, B. W. Pogue, and K. D. Paulsen, "Image guided diffuse optical fluorescence tomography implemented with Laplacian-type regularization," *Opt. Express* **15**(7), 4066–4082 (2007).
20. H. Dehghani, M. E. Eames, P. K. Yalavarthy, S. C. Davis, S. Srinivasan, C. M. Carpenter, B. W. Pogue, and K. D. Paulsen, "Near infrared optical tomography using NIRFAST: algorithm for numerical model and image reconstruction," *Commun. Numer. Methods Eng.* (2008), doi: 10.1002/cnm.1162.